Earth Syst. Sci. Data, 9, 589–600, 2017
https://doi.org/10.5194/essd-9-589-2017


Open Access Earth System Science Data

# Multibeam bathymetry and CTD measurements in two fjord systems in southeastern Greenland

**Kristian Kjellerup Kjeldsen[1,2,3], Reimer Wilhelm Weinrebe[4], Jørgen Bendtsen[5,6], Anders Anker Bjørk[1,7,8], and Kurt Henrik Kjær[1]**

[1]Centre for GeoGenetics, Natural History Museum, University of Copenhagen, 1350 Copenhagen K, Denmark
[2]Department of Earth Sciences, University of Ottawa, Ottawa, K1N 6N5, Canada
[3]DTU Space – National Space Institute, Technical University of Denmark, Department of Geodesy, 2800 Kgs. Lyngby, Denmark
[4]GEOMAR, Helmholtz-Zentrum für Ozeanforschung, 24148 Kiel, Germany
[5]Arctic Research Centre, Aarhus University, 8000 Aarhus, Denmark
[6]ClimateLab, Symbion Science Park, Fruebjergvej 3, 2100 Copenhagen Ø, Denmark
[7]Department of Earth System Science, University of California, Irvine, CA 92697, USA
[8]NASA Jet Propulsion Laboratory, Pasadena, CA 91109, USA

*Correspondence to:* Kristian Kjellerup Kjeldsen (kkjeldsen@snm.ku.dk)

Received: 7 April 2017 – Discussion started: 20 April 2017
Revised: 11 July 2017 – Accepted: 14 July 2017 – Published: 18 August 2017

**Abstract.** We present bathymetry and hydrological observations collected in the summer of 2014 from two fjord systems in southeastern Greenland with a multibeam sonar system. Our results provide a detailed bathymetric map of the fjord complex around the island of Skjoldungen in Skjoldungen Fjord and the outer part of Timmiarmiut Fjord and show far greater depths compared to the International Bathymetric Chart of the Arctic Ocean. The hydrography collected shows different properties in the fjords with the bottom water masses below 240 m in Timmiarmiut Fjord being 1–2 °C warmer than in the two fjords around Skjoldungen, but data also illustrate the influence of sills on the exchange of deeper water masses within fjords. Moreover, evidence of subglacial discharge in Timmiarmiut Fjord, which is consistent with satellite observations of ice mélange set into motion, adds to our increasing understanding of the distribution of subglacial meltwater. Data are available through the PANGAEA website at https://doi.pangaea.de/10.1594/PANGAEA.860627.

## 1 Introduction

During the past decades the Greenland ice sheet has experienced a considerable increase in mass loss associated with the speeding up of glaciers and enhanced melting (Khan et al., 2015). An anomalous inflow of subtropical waters driven by atmospheric changes, multidecadal natural ocean variability, and a long-term increase in the North Atlantic's upper ocean heat content since the 1950s has, in conjunction with increased meltwater runoff, led to enhanced submarine melting. This is believed to have triggered the retreat of Greenland's outlet glaciers, partly responsible for the increased ice loss (Straneo and Heimbach, 2013).

In order to better understand oceanic, cryospheric, and geological processes and their interaction, detailed knowledge of the morphology of a given survey area is essential. The International Bathymetry Chart of the Arctic Ocean (IBCAO; Jakobsson et al., 2012) provides an overview of the circum-Arctic bathymetry. However, in many of the Greenland fjord systems there is little, if any, bathymetric information, and therefore the resulting gridded bathymetry may have large errors. Narrow fjords, bays, or islands only slightly wider than the IBCAO resolution (500 m) are difficult to preserve, yet this is at least partly aided by including land topography, which in Greenland is based on a 2000 × 2000 m resolution digital elevation model (DEM; Jakobsson et al., 2012). As a

result, many glaciers appear grounded near or at sea level, whereas in reality the glaciers are grounded in deeper waters (Andresen et al., 2014; Rignot et al., 2016).

The publication of different datasets is continuously improving the bathymetry around Greenland (e.g., Arndt et al., 2015; Fenty et al., 2016; Rignot et al., 2015, 2016; Schumann et al., 2012; Williams et al., 2017), even if it is only based on a suite of single-point observations (Andresen et al., 2014) or inversion of gravity data to obtain bathymetry (Porter et al., 2014). Whereas the topography of the onshore area is more easily determined from air and satellite imagery and altimetry (e.g., Korsgaard et al., 2016; Willis et al., 2015), the relief of the submarine parts is hidden by the water column and can only be determined with hydroacoustic methods or aerial gravimetry. Thus, extensive bathymetric mapping is necessary to create a full image of the seafloor morphology.

During the summer of 2014 a multibeam echo sounder was temporarily installed on SS *ACTIV* (Fig. 1) and used to map the seafloor in two fjord systems in southeastern Greenland. To obtain knowledge of the water column, sound velocity profiles were determined at 11 positions using a CTD sensor (CTD: conductivity, temperature, depth). The data presented here supplement data acquired during the 2016 field campaign of Oceans Melting Greenland (Fenty et al., 2016) and as a consequence enabled better use of the ship's resources during the 2016 campaign.

**Figure 1.** The three-masted wooden schooner SS *ACTIV*.

### Study site

The study area consists of two fjord systems in southeastern Greenland, namely Timmiarmiut Fjord and the fjord systems around Skjoldungen (Fig. 2b). Timmiarmiut Fjord (Fig. 2c) is ca. 57 km long and reaches the Timmiarmiut Glacier, a large marine outlet glacier from the ice sheet. Along the fjord there are different branches and islands of variable sizes, in particular towards the north where the fjord system reaches Heimdal Glacier, another large marine outlet glacier from the ice sheet. Both glaciers are fast-moving outlets of the Greenland ice sheet (Rignot and Mouginot, 2012), with Timmiarmiut Glacier being the 15th fastest in Greenland. The fjord system also drains a large number of smaller glaciers and ice caps, both land- and marine-terminating, that are either isolated or in contact with the ice sheet. At the fjord mouth, depths extent down to ca. 620 m according to IBCAO (Jakobsson et al., 2012). These depths are based on single-beam echo soundings retrieved from the Olex database (http://www.olex.no) as the median values on a $0.12 \times 0.12$ arcmin grid. Subsequently, these have been filtered onto a $2 \times 2$ km grid using the median $z$ value within each grid cell before being resampled to a $500 \times 500$ m grid and evaluated (Jakobsson et al., 2012). The fjord system surrounding Skjoldungen (Fig. 2d) is comprised of a northern and a southern sound, Nørre Skjoldungesund (NSsund; ca. 49 km) and Søndre Skjoldungesund (SSsund; ca. 52 km), respectively, and a narrow, shallow section (ca. 10 km) towards the northwest that links the two sounds. The fjord system drains both local and ice sheet glaciers and ice caps with the vast majority being land-terminating, while the large ice-sheet-based Thrym Glacier enters the fjord directly in the very northwestern part of the fjord system at the head of NSsund. Around Skjoldungen the official nautical chart supplied by the Danish Geodata Agency is comprised of low-density point depth measurements ranging between 179 and 548 m in NSund and between 46 and 702 m in SSsund, while for both NSsund and SSsund IBCAO suggests depths down to ca. 20 m. The Fjord system around the island of Skjoldungen is annually visited by cruise ships, thus adding to the importance of mapping the fjords.

Outside the fjord systems, oceanographic conditions are dominated by the East Greenland Coastal Current (EGCC) above the shelf and the East Greenland Current (EGC) located at the shelf break (Sutherland and Pickart, 2008). These drive polar surface water originating from the Arctic Ocean and Atlantic water originating from the Irminger Sea.

## 2 Data and methods

The data in this study were collected during July 2014 and are comprised of a multibeam dataset and 11 CTD profiles. Below follows a description of the system, sensors and components, and the deployment. Figure 3 shows the deployment of the system onboard SS *ACTIV*. The software used for data acquisition was ELAC Nautik Hydrostar 3.5.3, while post-processing was accomplished using the software packages ELAC Nautik HDPpost and CARIS HIPS as well as the open-source software packages MB-System (Caress and Chayes, 1996) and GMT (Wessel and Smith, 1991).

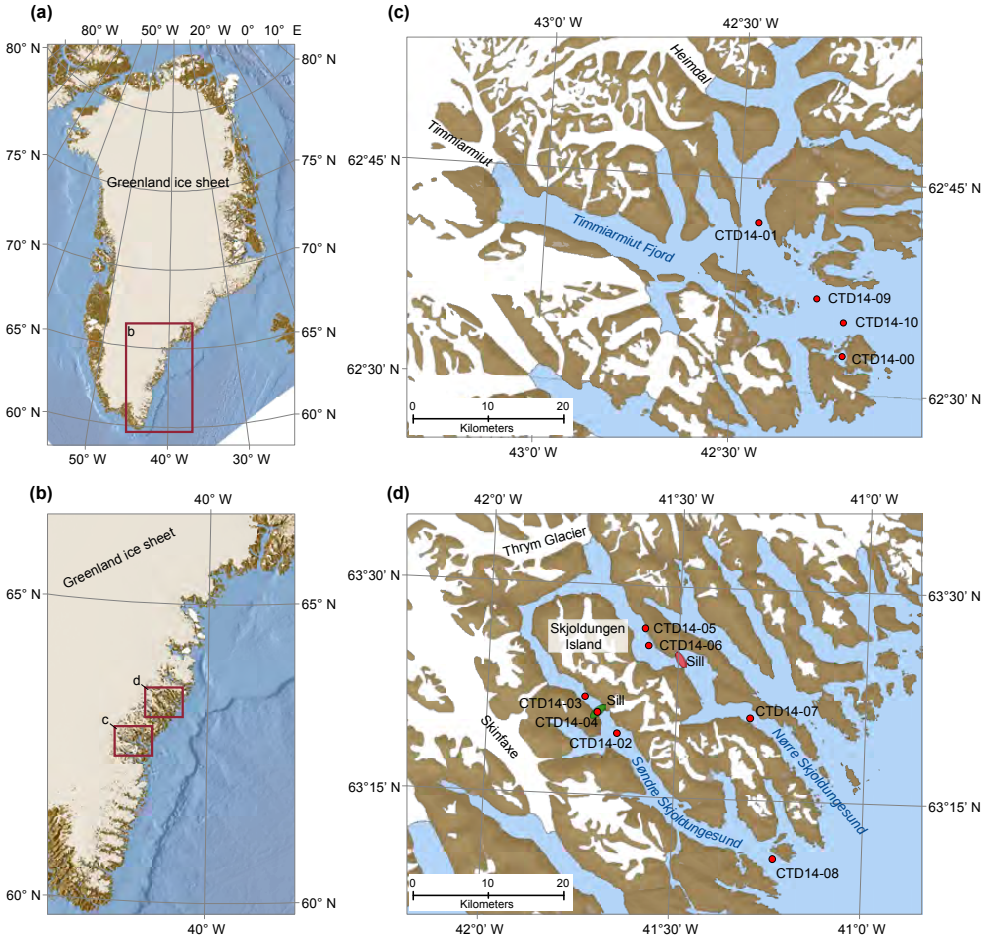


**Figure 2.** Maps of Greenland **(a)** and the southeast coast **(b)** with red boxes show location of the study sites. Map of the Timmiarmiut Fjord system **(c)** and the fjord complex around Skjoldungen **(b)** with Nørre Skjoldungesund (NSsund) towards the north and Søndre Skjoldungesund (SSsund) towards the south **(d)**. Note the location of two sills found in NSsund and SSsund. Also shown in **(c–d)** are the locations of the CTD stations.

## 2.1 Seabeam 1050

Multibeam systems are echo sounders that map the seafloor along a wide swath beneath the vessel. Due to their complexity, such systems are generally permanently installed in the hull of survey vessels. Onboard SS *ACTIV* we temporarily installed a portable ELAC Nautik Seabeam 1050 multibeam system provided by the GEOMAR Helmholtz-Centre for Ocean Research Kiel.

The Seabeam 1050 multibeam echo sounder collects bathymetry data with beams as narrow as $1.5° \times 1.5°$ and a swath width of up to 153°. The 50 kHz signal achieves a depth range of more than 2000 m. Different to other multibeam systems, which transmit a full swath of acoustic energy and use directed reception (beam forming), the Seabeam 1050 applies beam forming at transmission and reception, thus achieving a very high side lobe suppression of 36 dB with very low error rates. The disadvantage of this technique is a slightly lower ping rate. The system is completely stabilized for roll of the ship if an adequate motion sensor is installed. The Seabeam 1050 employs two transducer arrays, port and starboard, both capable of transmitting and receiving. Their acoustic planes are tilted 38° to the vertical. The arrays are normally installed fixed to the ship's hull, but on SS *ACTIV* they were mounted using a steel pole over the port side of the vessel. An overview of the technical specifications of the Seabeam 1050 is provided in Table 1.

## 2.2 Navigation, heading, and motion sensor F180R

The F180R inertial attitude and positioning system from Coda Octopus is an instrument designed to make precise measurements of the vessel attitude (including heading), dynamics, and geographical position for use in any marine hydrographic survey application. It is a multisensor system consisting of two survey-grade GPS receivers and an inertial measurement unit (IMU) made up of three solid-state gyros and three inertial-grade accelerometers. The IMU of the

**Table 1.** Overview of the technical specifications of the Seabeam 1050.

| | |
|---|---|
| Frequency: | 50 kHz |
| Maximum depth: | 3000 m |
| Beam width: | 1.5° × 1.5° |
| Pulse length: | 0.15–10 ms |
| Side lobe suppression: | 36 dB (transmission and reception) |
| Maximum swath width: | 153° |
| Maximum number of beams: | 126 |
| Beam spacing: | equiangular |

**Table 2.** Performance specifications of the F180R system.

| | According to specifications | Achieved during *ACTIV* survey |
|---|---|---|
| Heading accuracy | 0.05° | 0.46° |
| Attitude accuracy | 0.025° | 0.045° |
| Position accuracy | 0.5 m (without DGPS DGPS or RTK) | 0.49 m |
| Heave accuracy | 5 % of heave amplitude, minimum 5 cm | Not determined |

F180R is built into a separate waterproof pod in order to allow the IMU to be located close to the transducer heads. The F180R integrates the information provided by the attitude and position sensors and takes advantage of their complementary attributes to yield a position and attitude solution more stable than either system operating in isolation. The performance specifications of the F180R system are provided in Table 2.

The F180R system performance depends on a variety of external factors, e.g., poor GPS satellite constellation and multipaths of the GPS signals that cause errors and reduced accuracy of attitude and heading determinations.

## 2.3 CTD sensor Sea & Sun CTD48M

The CTD48M (Sea & Sun Marine Tech) memory probe is a small (1.2 kg) microprocessor-controlled multi-parameter titanium (except screws) probe for precise marine measurements. The accuracy of the conductivity and temperature sensor is specified as $\pm 0.003\,\mathrm{mS\,m^{-1}}$ and $\pm 0.002\,^{\circ}\mathrm{C}$, respectively. Considering the instrumental drift we estimate the temperature and salinity error to be about $\pm 0.05\,^{\circ}\mathrm{C}$ and $\pm 0.05$, respectively. This is well below the temperature and salinity range in the water column reported below. The CTD48M data acquisition rate was set to record data every 1 dbar during both downcast and upcast. CTD profiles were obtained manually using rope and a diving lead. Practical salinity ($S_P$) was calculated by the Sea & Sun Marine Tech software and potential temperature was calculated from IOC et al. (2010). Only downcast profiles were considered in the analysis.


**Figure 3.** Deployment of the multibeam system onboard SS *ACTIV* using a clamp and a U-shaped clip **(a-b)**. **(c)** The system during the surveying mode and **(d)** the system in the safe position used for transit. The multibeam system and computers were in installed in the wheelhouse **(e)**.

## 2.4 System installation onboard *ACTIV*

The two multibeam transducers were mounted to a 6 m pole, which was attached to the hull outboard at the port side midship using a clamp and a U-shaped clip (Fig. 3a, b). The transducer head was secured by two Dyneema ropes attached to the vessel (Fig. 3c). During transit and in ice-covered areas, the entire pole could be hoisted up into a safe position (Fig. 3d). The construction was sufficiently stable and easy to manage throughout the entire cruise; however, the hydrodynamic pressure of the water against the pole during the surveys caused a slight bending of the pole. In addition, a collision with an ice floe on 22 July might have also shifted the transducers slightly out of position. Both events likely had an influence on the accuracy of the multibeam data. The multibeam system and the computer for data acquisition were installed in the wheelhouse (Fig. 3e).

The IMU of the motion sensor F180R was installed on the deck close to the transducer pole. The two GPS antennas were mounted at a distance of 2.003 m apart on a wooden bar, which was temporarily installed on top of the wheelhouse. The motion sensor was set up to determine the motion of the vessel at the positions of the multibeam transducers (remote lever arm calculation). The reference point for the multibeam depth measurements was defined to be a point exactly above the center point of the transducers at water level.

### 2.5 Post-setup calibration and limitations

Once the temporary installation was completed, several components of the system had to be calibrated. The motion sensor F180R runs a self-calibration scheme, which requires considerable movement of the vessel and a continuously good GPS signal. Initially, the self-calibration failed. After remounting the GPS antennas at a position near the stern of the vessel to reduce the multipath of the GPS signals caused by the masts and rig, a new self-calibration procedure of the F180R was performed. At this position a stable operation of the motion sensor was achieved; however, the accuracy of the attitude and heading determinations missed the attainable specifications (Table 2).

The multibeam system requires calibration to determine the angular offsets of the transducers from the horizontal (roll offset) and the vertical (pitch offset) axis, respectively. To perform a roll calibration, a profile of multibeam data over an essentially flat seafloor is recorded on the same line in both directions. When both lines are processed separately, a potential roll offset will lead to different inclinations of the seafloor in the recorded data and the angular offset can be determined. To determine a possible pitch offset, a structure on the seafloor is mapped on two lines in opposite directions along the same profile. A possible pitch offset leads to different positions of the structure in separately processed lines. As no information on the seafloor depth was available beforehand, the calibrations had to be run over "unknown" seafloor. It turned out that the area was not well suited for a roll calibration; however, an estimate of the roll offset of 0.6° could be determined from the recordings and was used during the following days. A significant vertical offset of the transducers had not been detected, so the pitch bias was set to 0°.

The slight bending of the pole likely influenced the accuracy of the multibeam data. We assume that the offset in angle from the vertical was within a few degrees, and as a 4° offset at a water depth of 1000 m increases the depth by 2.4 m and also shifts the horizontal position of the measured point by 70 m, we anticipate that the uncertainty related to the bending and collision was within a few meters. However, as the system was only temporally installed and the seafloor "unknown", we were unable to test how our setup was affected.

## 3 Results and discussion

### 3.1 Multibeam surveys

The multibeam system was installed onboard *ACTIV* on 15 July 2014 when the vessel was anchored in the fjord south of the old Timmiarmiut weather station. Multibeam surveys were carried whenever weather and ice conditions as well as the scientific program allowed until the system was dismounted on the evening of 28 July 2014. The total track length of the multibeam surveys was 402 km recorded in 54.86 h and based on a total of 74 502 pings.

#### 3.1.1 Timmiarmiut area survey

Multibeam surveys in the Timmiarmiut area were carried out on 16, 17, 18, and 28 July. The days of 16 and 17 July were used to calibrate the setup and reconfigure the original installation. The survey in the Timmiarmiut Fjord area was continued on 18 and 28 July; however, due to numerous ice floes and icebergs only a part of the fjord was mapped (Fig. 4a). The survey shows that at least the outer part of the fjord consists of depths down to ca. 1060 m. An enlargement of the mouth of Timmiarmiut Fjord is provided in Fig. 5a. At a cross section at the fjord mouth, the deepest part is found along a ca. 2 km wide section in the middle where depths range between 740 and 830 m. North of this midsection, depths increase from ca. 780 to ca. 95 m over a distance of ca. 1.2 km. South of the midsection, depths increase from 780 to ca. 190 m over a ca. 2 km stretch intervened by a 1 km wide and ca. 150 m deep trough that extends down to ca. 550 m, which further up fjord increases to ca. 450 m. The general configuration of a wide, deep cross section with great depths is characteristic of the outer well-surveyed area, which covers ca. 15 km from the mouth and up fjord, but it also seems to resemble the branch towards the north covered by the red line in Fig. 4a despite the poorer multibeam coverage. In order to compare to existing data, we extract data from the deepest part of the fjord in the along-fjord direction (Fig. 4b, black and red lines), which ranges between ca. 800 and 880 m. Figure 4b shows data extracted from IBCAO (Jakobsson et al., 2012) along the three center lines: dashed red, solid red, and black. Our new data show that along the surveyed center line, the fjord is on average 325 m deeper where data overlap. Note that along the inner part of the fjord (dashed red line), IBCAO contains values above sea level. Following our data collection in 2014, the NASA-led Oceans Melting Greenland (OMG) mission (Fenty et al., 2016) acquired data in Timmiarmiut Fjord during their 2016 cruise. With knowledge of our data, OMG was able to collect data to supplement our mapping effort, thus saving time and enabling better use of the ship's resources.

#### 3.1.2 Skjoldungen Fjord survey

In the Skjoldungen Fjord complex around Skjoldungen, the multibeam system was deployed on 20, 21, 22, 23, 24, and 26 July. Nearly the entire fjord area was surveyed, leaving only a small gap of 5 km in the innermost part of the fjord system and small unmapped stripes close to the shorelines. Whenever possible, the fjord was mapped along three lines: one in the center, one closer to the northern shore, and one closer to the southern shore. The innermost stretch of the fjord area could not be mapped as the slopes of the surrounding mountains were too steep for the motion sensor to main-

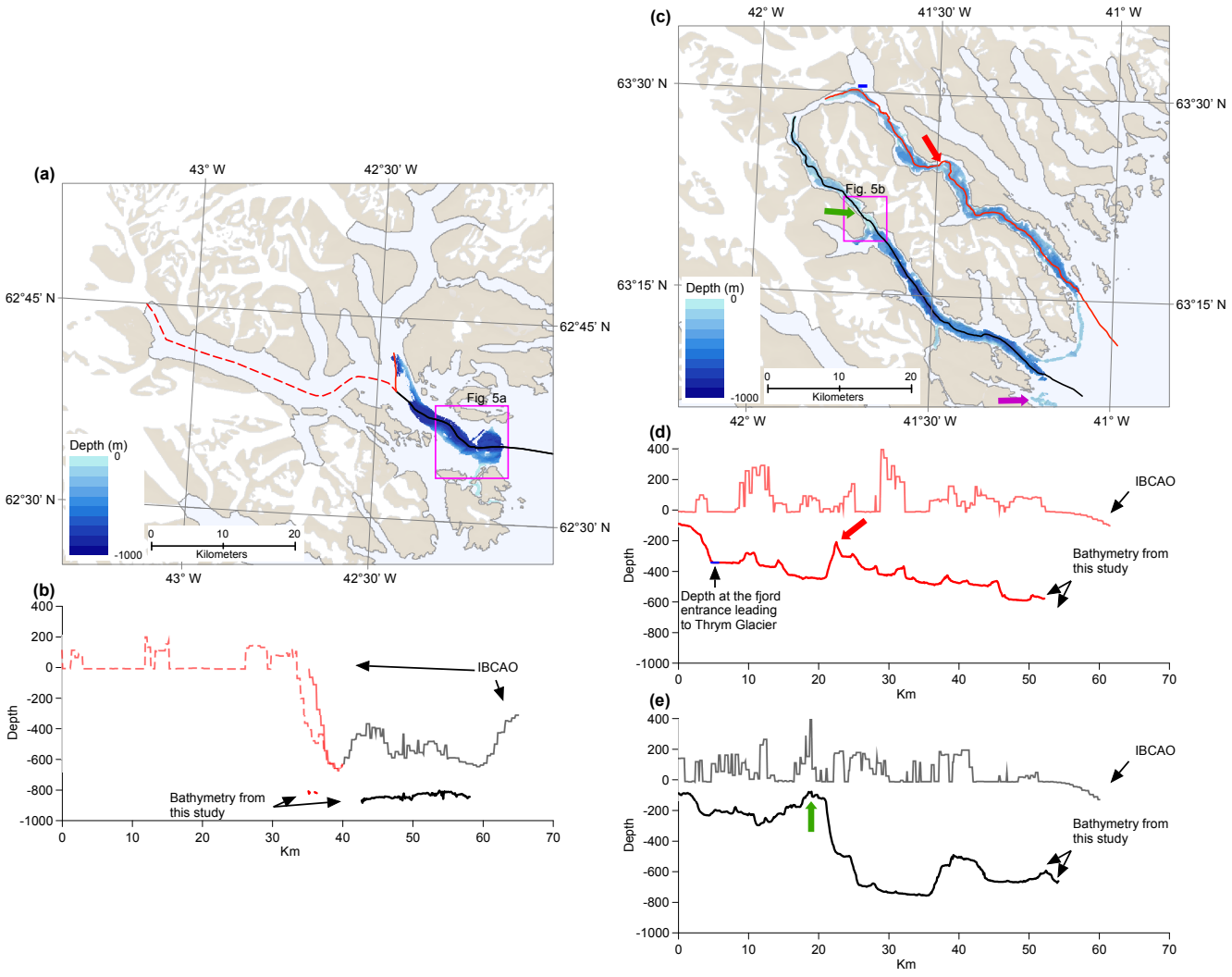


**Figure 4.** Surveyed bathymetry in the Timmiarmiut Fjord system **(a)**. The three colored lines follow the deepest part along the fjords and are illustrated in panel **(b)**, representing the outer well-surveyed area (black line), the branch towards the north leading to Heimdal Glacier at the head, and towards Timmiarmiut Glacier (dashed red line). The surveyed bathymetry around Skjoldungen is illustrated in panel **(c)**, while panel **(d)** shows the longitudinal profiles of Søndre Skjoldungesund (black lines) and Nørre Skjoldungesund (red lines). Green, red, and magenta arrows in panels **(c)** and **(d)** indicate the prominent sill in SSsund, the local high in NSsund, and the offshore shoal, respectively. For the profiles in panels **(b)** and **(d)**, bathymetry obtained from IBCAO is included.

tain its GPS connection; thus the multibeam system lacked navigation, heading, and motion information. Besides this small gap, a comprehensive map of the entire Skjoldungen Fjord area can now be presented for the first time (Fig. 4c). Figure 4d shows the bathymetry from our new data and IBCAO-extracted data at the center lines of the two fjords. Note that the IBCAO dataset here contains values above sea level.

Generally, the fjord width around Skjoldungen varies between 1.1 and 3.1 km except for a narrow stretch along SSsund, where the fjord width narrows down to ca. 600 m, and along a small stretch along the innermost unmapped part, where the width narrows down to ca. 580 m.

The bathymetry map of the Skjoldungen Fjord complex displays water depths up to 800 m (Fig. 4c and d). The deepest part is a stretch of about 10 km in SSsund. Generally, the southern fjord features an outer deep part showing water depths between 500 and 800 m and a shallow inner part with depths never reaching more than 300 m. Between the outer and inner parts along the narrowing of the fjord, there is a prominent sill with depths only extending down to ca. 77 m (green arrow, Fig. 4c, d; an enlargement is provided in Fig. 5b). Interestingly, in the field we observed multiple lateral moraines on land on either valley side dipping concave down towards the sill or near it. On digital elevation models and orthophotos from 1981 (Korsgaard et al., 2016), the

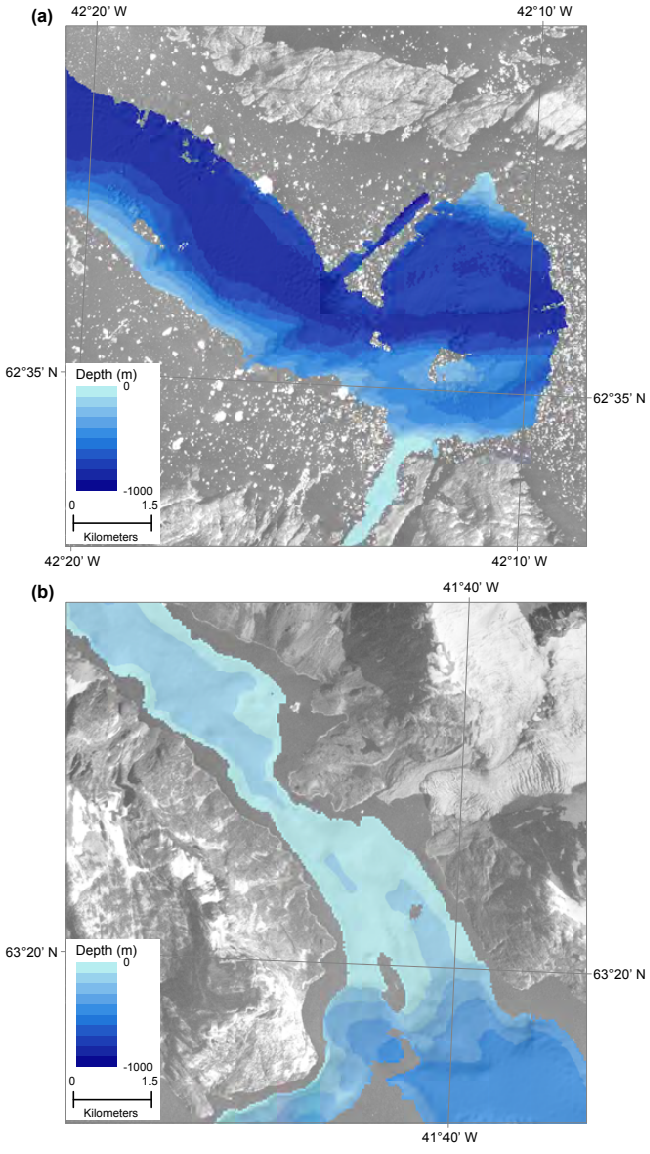


**Figure 5.** Enlargement of the mapped bathymetry at the mouth of Timmiarmiut Fjord **(a)** and around the sill region in SSsund **(b)**. Both maps overlay a 1981 orthophoto derived from aerial imagery.

lateral moraines are detectable; however, the actual structure and extent of the moraines is difficult to assess. The age of these moraines has yet to be determined, but their presence suggests that the sill and bedrock outcrop that forces the narrowing of the fjord acted as a pinning point for the receding glacier during deglaciation of the fjord.

The bathymetry of the NSsund is remarkably different from the bathymetry of the SSsund. NSsund shows a more gradual increase of water depths from 85 m in the very inner part to ca. 590 m at the entrance with a few undulations along the fjord and a local high of ca. 210 m (red arrow, Fig. 4c, d). However, in the vicinity of this local high point, only part of the area was surveyed and therefore a deeper path in the non-surveyed area of the bend could be possible, thus making our data a minimum estimate of the limiting depth of NSsund. At the fjord entrance leading to Thrym Glacier the water depth in NSsund is ca. 340 m (blue bar, Fig. 4c, d).

In the non-surveyed area in the northwestern part of the fjord complex where SSsund and NSsund are connected, water depth is likely limited and perhaps the deepest points in either end reflected the maximum depth. However, a moraine complex marking the Little Ice Age maximum extent of a local glacier originating from Skjoldungen extends halfway into the fjord and likely causes the fjord to be fairly shallow.

Around the island of Skjoldungen, IBCAO (Jakobsson et al., 2012) displays only a limited number of grid cells with negative values. Along the longitudinal profile overlapping data from this study and IBCAO range between 15 and 390 m with an increase in depth out on the shelf (Fig. 4d). The values above sea level in the IBCAO dataset, both around Skjoldungen and in Timmiarmiut Fjord, are in part due to the 500 $\times$ 500 m resolution of the data not fully being capable of resolving narrow fjords, but more likely data not being available or incorporated into the final dataset.

Offshore of the Skjoldungen fjord complex, we further surveyed a small shoal (magenta arrow, Fig. 4b). At the position 63°07.5′ N, 41°11.0′ W a very shallow area was mapped; the seafloor at this position showed water depths as shallow as 13 m. Surveying along two additional profiles, the extent of this feature could be outlined; unfortunately, an iceberg was stranded right on the shallowest position, so this spot could not be mapped. This submarine feature has dimensions of ca. 800 $\times$ 400 m and a height of ca. 200 m.

### 3.1.3 Constraints and limitations of the multibeam survey

The part of the area mapped during the SS *ACTIV* cruise in 2014 has never been surveyed before using a multibeam system. Furthermore, for great parts of the region no sounding information was available at all. The conditions for multibeam surveys in this area, particularly on this cruise, were difficult and of course this has affected the quality of the data.

Multibeam transducers are usually permanently installed in the hull of a vessel. For precise measurements of the water depth, the transducers have to be mounted such that their three axes are aligned horizontally, vertically, and in the direction of the center line of the vessel. Minimal deviations are determined by a calibration scheme following the installation. On SS *ACTIV* the transducers were installed temporarily at the lower end of a pole 6 m in length, which was then mounted over the side of the vessel. Of course this cannot be as stable as an installation flush in the hull. The pole is prone to vibrations, and the hydrostatic pressure on the pole while deployed in the water and when moving led to slight bending of the pole. Floating ice in the water also collided with the pole, moving it slightly out of position. A proper survey would have required at least a roll calibration each time the

**Table 3.** Overview of the 11 CTD profiles.

| Station no. | Date (dd-mm-yyyy) | Fjord system | Latitude (degrees) | Longitude (degrees) | Depth of the CTD profile (m) | Water depth (m) |
|---|---|---|---|---|---|---|
| CTD14-00 | 16-07-2014 | TF | 62.52633 | −42.18650 | 14 | 56 |
| CTD14-01 | 18-07-2014 | TF | 62.69767 | −42.44867 | 707 | 795 |
| CTD14-02 | 21-07-2014 | SSsund | 63.32350 | −41.65467 | 420 | 454 |
| CTD14-03 | 21-07-2014 | SSsund | 63.36550 | −41.74217 | 135 | 161 |
| CTD14-04 | 21-07-2014 | SSsund | 63.34800 | −41.70750 | 75 | 59–90* |
| CTD14-05 | 22-07-2014 | NSsund | 63.44933 | −41.58950 | 13 | 13 |
| CTD14-06 | 23-07-2014 | NSsund | 63.42883 | −41.57967 | 412 | 420 |
| CTD14-07 | 23-07-2014 | NSsund | 63.34717 | −41.30383 | 323 | 407 |
| CTD14-08 | 24-07-2014 | SSsund | 63.18167 | −41.23200 | 238 | 238 |
| CTD14-09 | 28-07-2014 | TF | 62.61100 | −42.28933 | 673 | 826 |
| CTD14-10 | 28-07-2014 | TF | 62.58450 | −42.21767 | 289 | 400 |

* Water depth registered by the ship while obtaining the CTD profile.

pole was deployed into the water; however, the area was not well suited for a roll calibration, which should be run over absolutely planar seafloor. As an ad hoc solution, transit lines run in opposite directions roughly along the same line were used throughout the survey to check and correct the roll bias values.

The motion sensor F180R used during the survey needs a continuously good connection to GPS satellites, and this was very difficult to maintain inside the fjords. Thus, the achieved heading accuracies and motion information often failed to achieve the intended specifications, leading to decreased quality of the multibeam data. Other sources of error in the data are missing tidal information, frequent changes in the water sound velocity due to the influence of meltwater, and abrupt course changes of the vessel due to ice floes.

However, in spite of the aforementioned problems the results of the multibeam surveys clearly demonstrate that it is actually possible using a ship such as SS *ACTIV* and a temporary installation to achieve bathymetric maps of satisfactory quality, even under difficult conditions in remote areas.

### 3.2 CTD measurements

During the SS *ACTIV* cruise, the CTD was deployed 11 times (Table 3). Locations of the profiles are displayed in Fig. 2c and d. Two of the 11 profiles were obtained in shallow waters while the ship was anchored and only the top 13–14 m of the water column was sampled. Three CTD profiles were obtained from Timmiarmiut Fjord (TF), four from SSsund, and two from NSsund. Note that the vessel drifted during the recording of CTD14-03, causing the water depth to vary.

Figure 6 illustrates the temperature and salinity profiles and the corresponding temperature–salinity ($T$–$S$) plots from the nine deeper profiles, divided into those from Timmiarmiut Fjord (a, d), SSsund (b, e), and NSsund (c, f).

In Timmiarmiut Fjord (Fig. 6a and d) three profiles were recorded reaching depths between 285 and 700 m. The innermost profile was recorded on 18 July, roughly midway between the fjord mouth and Timmiarmiut and Heimdal glaciers, while the two other profiles were recorded 10 days later on 28 July closer to the fjord mouth. The three profiles show certain similarities but also differences, with the two outermost profiles being almost identical throughout the profiles. For all three profiles the top consists of a pronounced cold layer between ca. 120 and 30 m with temperatures less than 0 °C and underlying a relatively low-saline ($S < 32$) and warm surface layer. However, the transition to the layers below differs as CTD14-01 shows a gradual warming and increasing salinity from ca. 110 to ca. 175 m, while at the fjord mouth the same conditions are already reached at a depth of ca. 125 m. At ca. 240 m the three profiles again start to deviate, with the midway profile generally being cooler by more than 1 °C at some depths.

Interestingly, the top ca. 40 m of the water column in profile CTD14-01 shows a clear difference compared to the two other profiles near the fjord mouth. Here temperatures are cooler and more saline compared to the fjord mouth. This is a strong indication of mixing with subglacial water and therefore subglacial discharge from a tidewater outlet glacier in the fjord (Mortensen et al., 2013). Subglacial meltwater discharge causes a buoyant ascending plume near the glacier where meltwater is mixed with high-saline bottom water (Bendtsen et al., 2015), and thereby the salinity in the upper water column may increase significantly (Kjeldsen et al., 2014). Thus, we speculate that the high salinities observed in the layer between ca. 50 and 10 m at station CTD14-01 can be explained as subglacial water from a tidewater outlet glacier. This is further supported by satellite observation from the period before the CTD profile was measured. MODIS imagery from 10 to 22 July 2014 (Fig. 7) shows that a large pool of ice mélange near the calving front of Heimdal Glacier north of the CTD station 14-01 is set into motion and directed away from the terminus by 12 July. By 17 July a large area of the inner fjord is covered by ice reach-

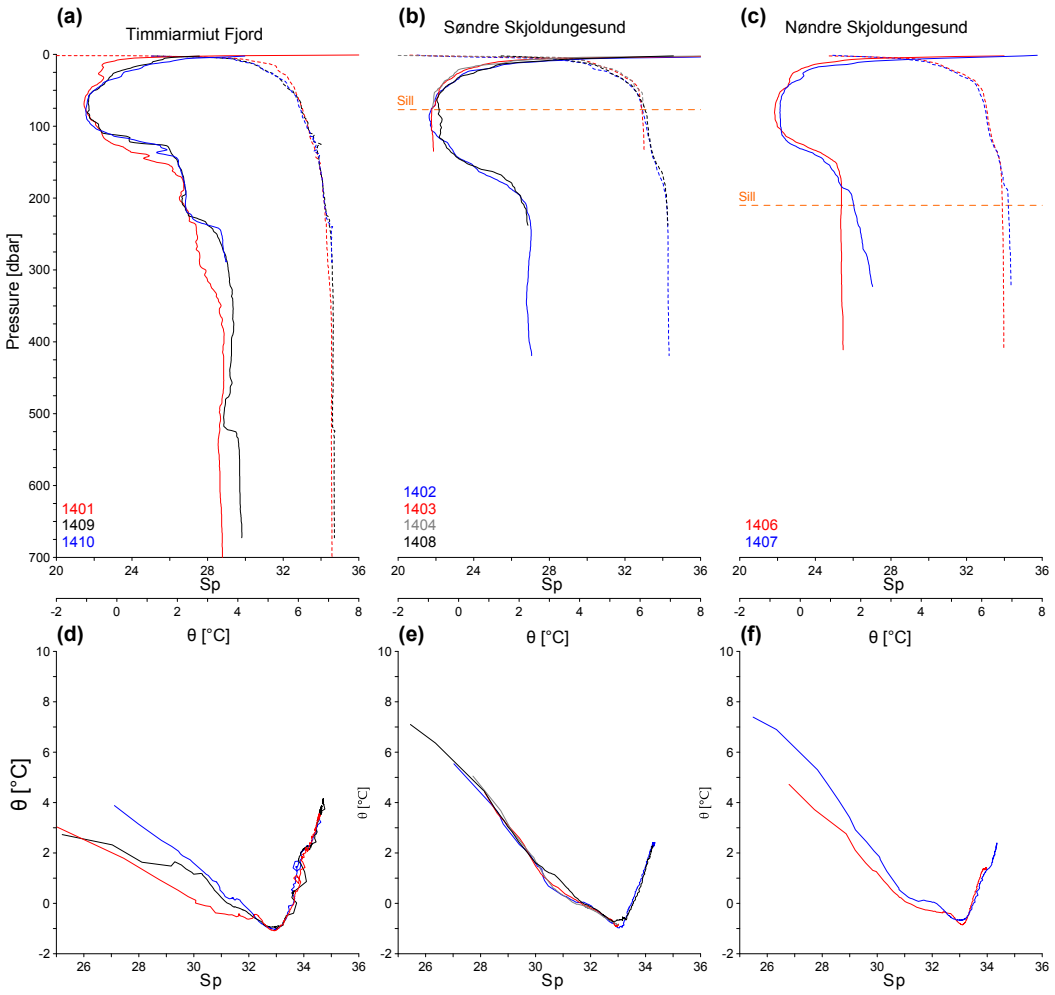


**Figure 6.** Temperature and salinity profiles and the corresponding $T$–$S$ diagrams for Timmiarmiut Fjord **(a, d)**, Søndre Skjoldungesund **(b, e)**, and Nørre Skjoldungesund **(c, f)**. Approximate sills depths retrieved from the bathymetry data are illustrated in **(b, c)**.

ing midway between Heimdal Glacier and the CTD station. Thus, the high salinities between 50 and 10 m of depth can be explained by subglacial water originating from the Heimdal tidewater outlet glacier, and the relatively low temperatures in the upper 50 m can be explained by heat loss due to the melting of the icebergs. However, the unsteady nature of these fjord systems can limit conclusions based on a few observations.

In SSsund four profiles (Fig. 6b and e) were recorded on 21 and 24 July, two seawards of the sill (CTD14-02 and CTD14-08; Fig. 4c, d, green arrow), one on the sill (CTD14-04), and one landwards of the sill (CTD14-03). The deepest reached 420 m and was recorded mid-fjord seawards of the sill, CTD14-02. Generally, the four profiles show the same properties down through the water column, with a fresh warm surface layer overlaying a layer of polar water that extends down to 200 m. Further below at greater depths, the water column appears homogenous with a constant temperature and salinity, though this is based only on a single profile that reaches 238 m (CTD14-08) and another that reaches 420 m (CTD14-02).

Interestingly, below ca. 110 m, profiles landwards and seawards of the sill begin to deviate from each other, with CTD14-03 (landwards) being ca. 0.6 °C cooler and 0.4 units more fresh. Possibly, this reflects a deeper-lying local water mass occupying the basin between the sill and the northwestern part of the fjord complex, as the inner part connecting SSsund and NSsund is likely shallow due the presence of a moraine complex, thus limiting the exchange of deeper water masses. This water mass would, however, likely be affected by water masses that flow just over the sill, possibly during winter and spring as observed in Godthåbsfjorden in western Greenland (Mortensen et al., 2011).

In NSsund (Fig. 6c and f) two deeper and one shallow profile were recorded. The shallow profile (CTD14-05) is omitted as it reassembles the nearby deeper profile, CTD14-06. The latter is recorded landwards of the sill (Fig. 4c, d, red arrow), while CTD14-07 was recorded midway between

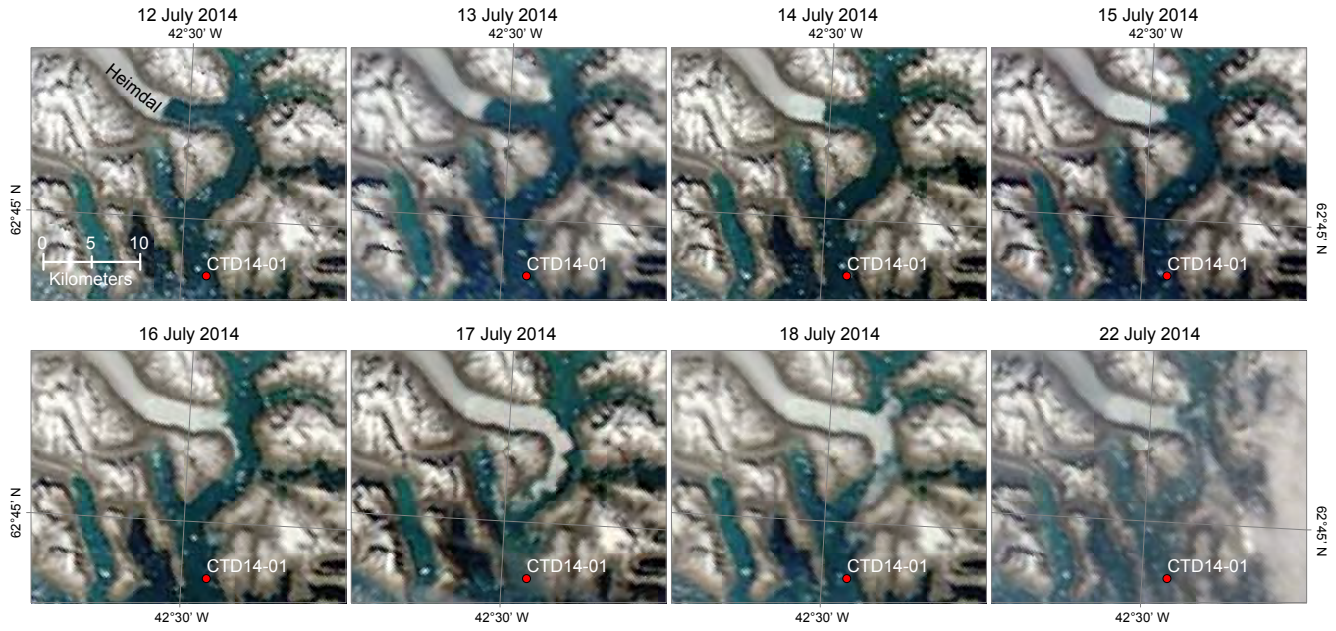


**Figure 7.** MODIS imagery of the inner part of the branch of Timmiarmiut Fjord that leads towards Heimdal at the head. The imagery illustrates the distribution of ice mélange set into motion on 13 July near the calving front of Heimdal Glacier due to the release of subglacial meltwater. During the following days the ice mélange expands and is directed southwards. In our CTD measurements on 18 July from CTD14-01, we detect this as a cooling and an increase in the salinity of the layer between 10 and 50 m of depth.

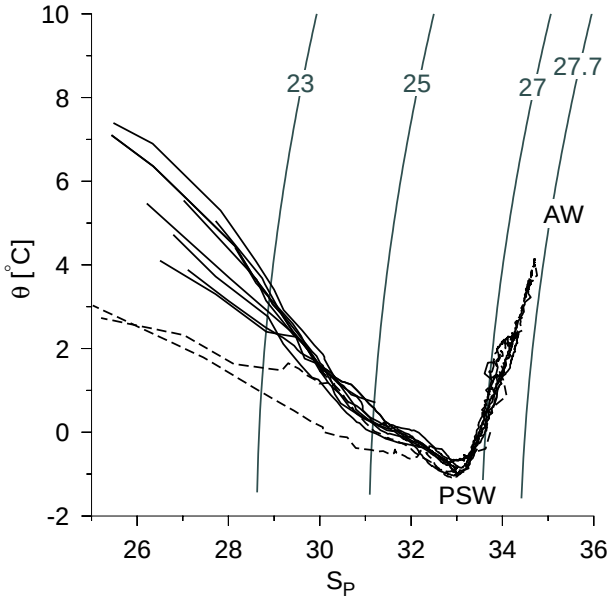


**Figure 8.** Potential temperature ($\theta$) and salinity ($S_P$) diagram of all profiles from the three fjords. The two stations in Timmiarmiut Fjord near the Heimdal tidewater outlet glacier (CTD14-01 and 14-09) are shown with dashed lines. Temperature–salinity characteristics of two water masses, i.e., Atlantic water (AW) and polar surface water (PSW), are indicated and lines of constant density ($\sigma_\theta$, $\mathrm{kg\,m^{-3}}$) are contoured.

the sill and the fjord mouth. In the uppermost part, the profiles look alike with CTD14-06 showing a slightly stronger stratification near 140 m, while at depth the deviation between the two profiles starts to become more obvious. Below ca. 185 m CTD14-07 gradually becomes warmer and more saline through to the deepest measurement at 323 m. In contrast, below ca. 185 m CTD-1406 remains unchanged with depth. This difference reflects limited water exchange in the deeper parts of the fjord, and thus supports the presence of a sill in accordance with the recorded bathymetry.

Relatively cold water masses characterize the three fjords in the upper ca. 120 m and, except for the presence of subglacial water in the innermost profile in Timmiarmiut Fjord, which has a local origin, the upper water masses share the same temperature and salinity characteristics. The deeper part of the fjords show some differences; the bottom water masses below 240 m in Timmiarmiut Fjord are 1–2 °C warmer than in the other two fjords. This indicates a stronger influence from mixing with warmer water masses in Timmiarmiut Fjord. Also, it may partly reflect the absence of sills such that Atlantic water flows into the fjord unimpeded.

The regional oceanographic conditions outside the fjord systems are dominated by the East Greenland Coastal Current (EGCC) above the shelf and the East Greenland Current (EGC) located at the shelf break (Sutherland and Pickart, 2008). The shelf is ca. 200–300 m deep outside the fjords and ca. 40–50 km wide. Upper water masses on the shelf are characterized by polar surface water ($\theta < 0\,^\circ\mathrm{C}$, $\sigma_\theta < 27\,\mathrm{kg\,m^{-3}}$;

Sutherland and Pickart, 2008) originating from the Arctic Ocean and influenced by melted ice and runoff. The Atlantic water is located on the shelf break and originates from the Irminger Sea and from recirculated water from the North Atlantic Current. Bottom water masses inside the fjords are relatively cold and from the temperature–salinity diagram (Fig. 8) they are located at the mixing line between Atlantic water (AW; $4.5 < \theta < 6.5\,^{\circ}\mathrm{C}$, $34.8 < S_P < 35.0$) and PSW. Water masses below 120 m are relatively cold and below 4 °C, which indicates a limited exchange between the deeper part of the fjords and the warm Atlantic water mass. However, the relatively warm bottom water masses in Timmiarmiut Fjord compared with the two other fjords further north could indicate a larger influence from warm Atlantic water here. This could possibly be due to the relatively narrow width of the shelf outside the fjord, but also, at least partly, the absences of sills.

## 4 Data availability

Multibeam bathymetry and hydrographic data are available through the PANGAEA website https://doi.org/10.1594/PANGAEA.860627. Additional data used here include the International Bathymetric Chart of the Arctic Ocean (IBCAO) (Jakobsson et al., 2012), available from https://www.ngdc.noaa.gov/mgg/bathymetry/arctic/arctic.html, a digital elevation model and orthophotos derived from stereophotogrammetric imagery recorded in 1981 (Korsgaard et al., 2016), available from NOAA National Centers for Environmental Information https://doi.org/10.7289/V56Q1V72, and Moderate Resolution Imaging Spectroradiometer (MODIS) archive satellite imagery, available from http://earthexplorer.usgs.gov.

## 5 Conclusions

In this study we have presented bathymetric data obtained during a cruise in 2014 using a multibeam system temporarily installed on SS *ACTIV*. The data collected provide new insights into fjords with limited information of the bathymetry, but they also supplement subsequent large-scale data collection from the NASA OMG mission. The need for new data is evident when comparing to existing data, such as IBCAO or single-point measurements from nautical maps. These new efforts provide better spatial resolution and, importantly, also a better description of depths and the seafloor morphology. For instance, comparison to IBCAO shows not only greater depths (Fig. 4b), but also that the 2000 × 2000 m land DEM that is implemented in IBCAO and its final 500 m of spatial resolution is insufficient to properly distinguish between land and fjord in these narrow fjord settings. It is also likely that the single-point measurements from the nautical charts, for instance around Skjoldungen, were not included in IBCAO, leading to considerable discrepancy. However, with the single major objective of IBCAO being to provide a portrayal of the Arctic Ocean seafloor (Jakobsson et al., 2012), it is understandable that not all fjord complexes are as well resolved as offshore bathymetry based on extensive multibeam mapping. However, large-scale efforts, such as the NASA OMG mission measuring bathymetry (Fenty et al., 2016) and the synthetic bathymetry datasets (Williams et al., 2017), are beginning to shed new light on the configurations of fjords around Greenland.

The CTD measurements collected during the cruise provide information about the properties of the water column in relation to sound velocity and the bathymetrical mapping, but they also allow insight into the distribution of water masses in the different fjord settings. Here we find considerable difference between the water masses located in the three fjord settings, influenced not only by the local bathymetry, such that sills in SSsund and NSsund hinder the exchange of deeper, warmer water masses that might affect the marine-terminating Thrym Glacier at the head of the fjord and the variability in the influence of Atlantic water flowing on the shelf outside the fjords. The latter causes deeper water in Timmiarmiut Fjord to be warmer relative to the fjords around Skjoldungen further north and possibly also reflects the absence of sills. Moreover, high salinities are observed in the layer between ca. 50 and 10 m in the inner part of Timmiarmiut Fjord, suggesting the release of subglacier meltwater from Heimdal Glacier up fjord of the CTD station, which is consistent with satellite imagery that shows a large pool of ice mélange set into motion 5 days prior to our CTD measurements.

The observations presented in this study complement large-scale efforts to obtain knowledge about the bathymetry and hydrography in the fjords around Greenland, but they also add to our understanding of how subglacial meltwater is distributed in fjord systems and the impact on fjord circulation (Bendtsen et al., 2015; Kjeldsen et al., 2014). This is important for understanding how a future warming ocean will affect the stability of marine-terminating outlet glaciers.

**Acknowledgements.** We thank the GEOMAR Helmholtz-Centre for Ocean Research Kiel for graciously lending us their Seabeam 1050 multibeam system, Wärtsilä ELAC Nautik for lending us a transducer mounting frame, and Teledyne CARIS for providing the software CARIS HIPS. Moreover, we thank the crew onboard SS *ACTIV* for their help collecting the data during the field campaign. Kristian Kjellerup Kjeldsen acknowledges support from the Danish Council Research for Independent Research (grant no. DFF – 4090-00151). Anders Anker Bjørk was supported by the Danish Council for Independent Research (grant no. DFF – 610800469) and by the Inge Lehmann Scholarship from the Royal Danish Academy of Science and Letters.

Edited by: Michael E. Contadakis
Reviewed by: Ian Fenty and one anonymous referee

## References


Andresen, C. S., Kjeldsen, K. K., Harden, B., Nørgaard-Pedersen, N., and Kjær, K. H.: Outlet glacier dynamics and bathymetry at Upernavik, Geol. Surv. Den. Greenl., 31, 79–82, 2014.

Arndt, J. E., Jokat, W., Dorschel, B., Myklebust, R., Dowdeswell, J. A., and Evans, J.: A new bathymetry of the North-east Greenland continental shelf: Constraints on glacial and other processes, Geochem. Geophy. Geosy., 16, 3733–3753, https://doi.org/10.1002/2015GC005931, 2015.

Bendtsen, J., Mortensen, J., Lennert, K., and Rysgaard, S.: Heat sources for glacial ice melt in a west Greenland tidewater outlet glacier fjord: The role of subglacial freshwater discharge, Geophys. Res. Lett., 42, 4089–4095, https://doi.org/10.1002/2015GL063846, 2015.

Caress, D. W. and Chayes, D. N.: Improved processing of Hydrosweep DS multibeam data on the R/V *Maurice Ewing*, Mar. Geophys. Res., 18, 631–650, https://doi.org/10.1007/BF00313878, 1996.

Fenty, I., Willis, J. K., Khazendar, A., Dinardo, S., Forsberg, R., Fukumori, I., Holland, D., Jakobsson, M., Moller, D., Morison, J., Münchow, A., Rignot, E., Schodlok, M., Thompson, A. F., Tinto, K., Rutherford, M., and Trenholm, N.: Oceans Melting Greenland: Early Results from NASA's Ocean-Ice Mission in Greenland, Oceanography, 29, 72–83, https://doi.org/10.5670/oceanog.2016.100, 2016.

IOC, SCOR and IAPSO: The international thermodynamic equation of seawater – 2010: Calculation and use of thermodynamic properties, Intergovernmental Oceanographic Commision, UNESCO, Manuals and Guides, 56, 1–196, 2010.

Jakobsson, M., Mayer, L., Coakley, B. J., Dowdeswell, J. A., Forbes, S., Fridman, B., Hodnesdal, H., Noormets, R., Pedersen, R., Rebesco, M., Schenke, H. W., Zarayskaya, Y., Accettella, D., Armstrong, A., Anderson, R. M., Bienhoff, P., Camerlenghi, A., Church, I., Edwards, M., Gardner, J. V., Hall, J. K., Hell, B., Hestvik, O., Kristoffersen, Y., Marcussen, C., Mohammad, R., Mosher, D., Nghiem, S. V., Pedrosa, M. T., Travaglini, P. G., and Weatherall, P.: The International Bathymetric Chart of the Arctic Ocean (IBCAO) Version 3.0, Geophys. Res. Lett., 39, L12609, https://doi.org/10.1029/2012GL052219, 2012.

Khan, S. A., Aschwanden, A., Bjørk, A. A., Wahr, J., Kjeldsen, K. K., and Kjær, K. H.: Greenland ice sheet mass balance: a review, Rep. Prog. Phys., 78, 046801, https://doi.org/10.1088/0034-4885/78/4/046801, 2015.

Kjeldsen, K. K., Mortensen, J., Bendtsen, J., Petersen, D., Lennert, K., and Rysgaard, S.: Ice-dammed lake drainage cools and raises surface salinities in a tidewater outlet glacier fjord, west Greenland, J. Geophys. Res.-Earth, 119, 1310–1321, https://doi.org/10.1002/2013JF003034, 2014.

Korsgaard, N. J., Nuth, C., Khan, S. A., Kjeldsen, K. K., Bjørk, A. A., Schomacker, A., and Kjær, K. H.: Digital elevation model and orthophotographs of Greenland based on aerial photographs from 1978–1987, Scientific Data, 3, 160032, https://doi.org/10.1038/sdata.2016.32, 2016.

Mortensen, J., Lennert, K., Bendtsen, J., and Rysgaard, S.: Heat sources for glacial melt in a sub-Arctic fjord (Godthåbsfjord) in contact with the Greenland Ice Sheet, J. Geophys. Res., 116, C01013, https://doi.org/10.1029/2010JC006528, 2011.

Mortensen, J., Bendtsen, J., Motyka, R. J., Lennert, K., Truffer, M., Fahnestock, M., and Rysgaard, S.: On the seasonal freshwater stratifi cation in the proximity of fast-flowing tidewater outlet glaciers in a sub-Arctic sill fjord, J. Geophys. Res.-Oceans, 118, 1382–1395, https://doi.org/10.1002/jgrc.20134, 2013.

Porter, D. F., Tinto, K. J., Boghosian, A., Cochran, J. R., Bell, R. E., Manizade, S. S., and Sonntag, J. G.: Bathymetric control of tidewater glacier mass loss in northwest Greenland, Earth Planet. Sc. Lett., 401, 40–46, https://doi.org/10.1016/j.epsl.2014.05.058, 2014.

Rignot, E. and Mouginot, J.: Ice flow in Greenland for the International Polar Year 2008–2009, Geophys. Res. Lett., 39, L11501, https://doi.org/10.1029/2012GL051634, 2012.

Rignot, E., Fenty, I., Xu, Y., Cai, C., and Kemp, C.: Undercutting of marine-terminating glaciers in West Greenland, Geophys. Res. Lett., 42, 5909–5917, https://doi.org/10.1002/2015GL064236, 2015.

Rignot, E., Fenty, I., Xu, Y., Cai, C., Velicogna, I., Cofaigh, C., Dowdeswell, J. A., Weinrebe, W., Catania, G., and Duncan, D.: Bathymetry data reveal glaciers vulnerable to ice-ocean interaction in Uummannaq and Vaigat glacial fjords , west Greenland, Geophys. Res. Lett., 43, 2667–2674, https://doi.org/10.1002/2016GL067832, 2016.

Schumann, K., Völker, D., and Weinrebe, W. R.: Acoustic mapping of the Ilulissat Ice Fjord mouth, West Greenland, Quaternary Sci. Rev., 40, 78–88, https://doi.org/10.1016/j.quascirev.2012.02.016, 2012.

Straneo, F. and Heimbach, P.: North Atlantic warming and the retreat of Greenland's outlet glaciers, Nature, 504, 36–43, https://doi.org/10.1038/nature12854, 2013.

Sutherland, D. A. and Pickart, R. S.: Progress in Oceanography The East Greenland Coastal Current: Structure, variability, and forcing, Prog. Oceanogr., 78, 58–77, https://doi.org/10.1016/j.pocean.2007.09.006, 2008.

Wessel, P. and Smith, W. H. F.: Free software helps map and display data, Eos T. Am. Geophys. Un., 72, 441–446, 1991.

Williams, C. N., Cornford, S. L., Jordan, T. M., Dowdeswell, J. A., Siegert, M. J., Clark, C. D., Swift, D. A., Sole, A., Fenty, I., and Bamber, J. L.: Generating synthetic fjord bathymetry for coastal Greenland, The Cryosphere, 11, 363–380, https://doi.org/10.5194/tc-11-363-2017, 2017.

Willis, M. J., Herried, B. G., Bevis, M. G., and Bell, R. E.: Recharge of a subglacial lake by surface meltwater in northeast Greenland, Nature, 518, 223–227, https://doi.org/10.1038/nature14116, 2015.